HHS Public Access

Author manuscript

Cell Rep. Author manuscript; available in PMC 2018 May 24.

Published in final edited form as:

Cell Rep. 2018 April 24; 23(4): 1020–1033. doi:10.1016/j.celrep.2018.03.117.

Cardiac mTORC1 Dysregulation Impacts Stress Adaptation and Survival in Huntington's Disease

Daniel D. Child[1,2], **John H. Lee**[3], **Christine J. Pascua**[4], **Yong Hong Chen**[1], **Alejandro Mas Monteys**[1], and **Beverly L. Davidson**[1,2,5,*]

[1]The Raymond G. Perelman Center for Cellular and Molecular Therapeutics, The Children's Hospital of Philadelphia, Philadelphia, PA, USA

[2]The Perelman School of Medicine, The University of Pennsylvania, Philadelphia, PA, USA

[3]Department of Psychiatry and Biobehavioral Sciences, University of California Los Angeles, Los Angeles, CA, USA

[4]Division of Cardiology, The Children's Hospital of Philadelphia, Philadelphia, PA, USA

SUMMARY

Huntington's disease (HD) is a dominantly inherited neurological disorder caused by CAG-repeat expansion in exon 1 of *Huntingtin* (*HTT*). But in addition to the neurological disease, mutant HTT (mHTT), which is ubiquitously expressed, impairs other organ systems. Indeed, epidemiological and animal model studies suggest higher incidence of and mortality from heart disease in HD. Here, we show that the protein complex mTORC1 is dysregulated in two HD mouse models through a mechanism that requires intrinsic mHTT expression. Moreover, restoring cardiac mTORC1 activity with constitutively active Rheb prevents mortality and relieves the mHTT-induced block to hypertrophic adaptation to cardiac stress. Finally, we show that chronic mTORC1 dysregulation is due in part to mislocalization of endogenous Rheb. These data provide insight into the increased cardiac-related mortality of HD patients, with cardiac mHTT expression inhibiting mTORC1 activity, limiting heart growth, and decreasing the heart's ability to compensate to chronic stress.

Graphical abstract

*Correspondence: davidsonbl@email.chop.edu.

[5]Lead Contact

SUPPLEMENTAL INFORMATION

Supplemental Information includes Supplemental Experimental Procedures and six figures and can be found with this article online at https://doi.org/10.1016/j.celrep.2018.03.117.

AUTHOR CONTRIBUTIONS

D.D.C., J.H.L., and B.L.D. designed the studies. D.D.C., C.J.P., and J.H.L. performed the experiments, collected the data, and analyzed the results. D.D.C., J.H.L., and A.M.M. designed and cloned the plasmids. Y.H.C. designed and cloned the CT.AAV construct. D.D.C. and B.L.D. wrote the manuscript.

DECLARATION OF INTERESTS

B.L.D. is a founder of Spark Therapeutics and is on the SAB of Intellia Therapeutics and Sarepta Therapeutics. None of this work was sponsored by, or reagents developed or licensed to, any of these entities at the time of submission.

In Brief: Child et al. demonstrate that mTORC1 dysregulation is a key molecular mechanism in the Huntington's disease (HD) heart phenotype. Impaired cardiac mTORC1 activity in HD mouse models requires intrinsic mHTT expression and explains the limited adaptation to cardiac stress.

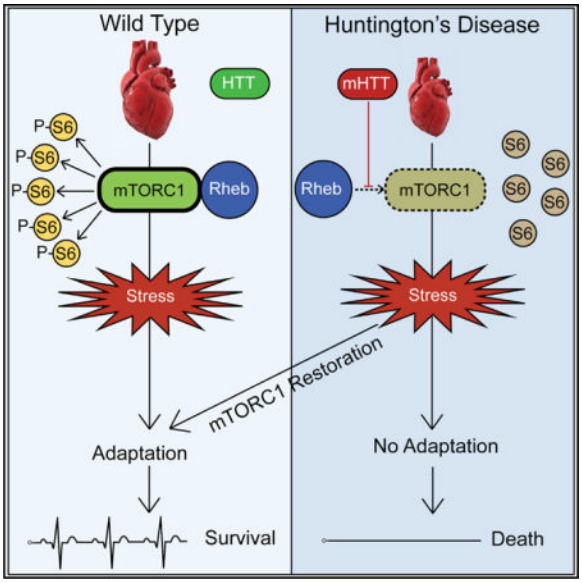

INTRODUCTION

Huntington's disease (HD) is a fatal, autosomal dominant neurodegenerative disease caused by CAG repeat expansion in exon 1 of the *huntingtin* gene. This mutation creates an expanded polyglutamine tract in the Huntingtin protein (HTT) and results in a mutant form of HTT (mHTT) that disrupts multiple cellular functions (The Huntington's Disease Collaborative Research Group, 1993). Pathologically, HD is characterized by profound neuronal death in the striatum and other brain regions (Rosas et al., 2001), which causes uncontrolled movements (chorea), behavioral abnormalities, and cognitive decline (Walker, 2007). Age of onset inversely correlates with CAG expansion length, and death occurs on average 10–15 years after symptom onset (Wexler et al., 2004). There is currently no cure for HD, but antisense oligonucleotide (ASO) and adeno-associated virus (AAV)-mediated gene therapies to reduce HTT levels in the CNS have demonstrated safety and efficacy in animal models and patients and are progressing in clinical trials (Boudreau et al., 2009; Ionis Pharmaceuticals, 2017; McBride et al., 2011; Stanek et al., 2013). However, HTT expression is ubiquitous (Li et al., 1993; Trottier et al., 1995), and HD affects peripheral tissues with high metabolic demand (Chaturvedi et al., 2010; Mihm et al., 2007; Ribchester et al., 2004). Thus, CNS-specific therapies may unmask peripheral HD phenotypes.

Heart disease is the second leading cause of death in HD patients across multiple populations (Lanska et al., 1988a, 1988b; Sørensen and Fenger, 1992), but the phenotype is still poorly understood. The few clinical studies that examined the heart in HD largely focused on neuronal inputs. Specifically, noninvasive, autonomic function analyses of sympathetic skin responses and heart rate variability measures suggested an abnormal balance between parasympathetic and sympathetic function, with HD patients tending to

experience decreased vagal activity and increased sympathetic tone (Bär et al., 2008; Kobal et al., 2004; Sharma et al., 1999). Epidemiological studies report a higher incidence of heart failure in HD patients compared to unaffected age-matched controls (Abildtrup and Shattock, 2013; CDC, 1994), and HD patient heart size is decreased at autopsy (Myers et al., 1998). A recent study specifically looking for cardiovascular disease risk factors found increased risk even in premanifest HD gene carriers (Bellosta Diago et al., 2018). However, the pathogenic mechanisms underlying these phenotypes have remained elusive and may include autonomic circuit degeneration within the CNS, intrinsic cardiac mHTT toxicity, and other systemic abnormalities.

In animal models, mHTT expression is associated with adverse cardiac phenotypes. Both *Drosophila* and mice engineered to express an expanded polyglutamine peptide in heart experience dilated chambers, impaired contractility, and reduced survival (Melkani et al., 2013; Pattison et al., 2008). The transgenic R6/2 and knockin Q150 HD mouse models have dilated ventricles and impaired cardiac function late in disease, coupled with fibrosis, increased apoptosis, altered ganglionic plexus morphology, and conduction abnormalities (Mielcarek et al., 2014b; Mihm et al., 2007; Wood et al., 2012). Cardiac gene expression networks in the R6/2 and Q150 models attribute heart pathology to altered neuronal or other systemic inputs (Mielcarek et al., 2014b). Additionally, the Q175 knockin HD mouse model displays abnormal heart rate variability and abnormal baroreceptor response, further implicating the autonomic nervous system's role in the HD heart phenotype (Cutler et al., 2017). However, hearts in R6/2 mice fail to hypertrophy when exposed to the β-adrenergic agonist isoprenaline (Mielcarek et al., 2014a), and impaired nucleotide metabolism suggests possible mitochondrial dysfunction (Toczek et al., 2016). Hearts in the full-length mHTT transgenic mouse, *BACHD*, exhibit impaired function, abnormal conduction, increased apoptosis, and fibrosis aggravated by isoprenaline treatment (Schroeder et al., 2016). Thus, mHTT expression may impart cardiotoxicity independent from CNS deficits, but mHTT's specific role in pathogenesis remains unknown.

One of the key regulators of heart size and stress responses is mechanistic Target of Rapamycin complex 1 (mTORC1), a serine-threonine kinase that integrates multiple environmental cues and promotes cellular growth and metabolism (Laplante and Sabatini, 2012). Abolishing mTORC1 activity by ablation of Rheb, the activating subunit of mTORC1, causes defective cardiovascular development (Goorden et al., 2011). Cardiac-specific Rheb knockout (KO) mice have reduced cardiac mRNA translation, retarded cardiomyocyte growth, and impaired cardiac function during the early postnatal period (Tamai et al., 2013; Zhang et al., 2010). mTORC1 activity is less critical for healthy adult hearts, but it plays a key role in mediating the heart's response to chronic stress. Cardiac-specific *raptor* deletion, an essential mTORC1 subunit, causes maladaptive responses to pressure overload, resulting in dilated cardiomyopathy and heart failure (Shende et al., 2011). Furthermore, rapamycin, a small molecule mTORC1 inhibitor, prevents cardiac compensation to volume and pressure overload and increases mortality in heart pathology models (Boluyt et al., 1997; Ikeda et al., 2015). Conversely, overexpression of mTORC1's catalytic subunit, mTOR, attenuates pressure overload-induced fibrosis and reduces inflammatory cytokine responses (Song et al., 2010). Accordingly, mTORC1 dysregulation in HD may explain the decreased heart mass and the increased mortality from heart disease.

Abnormal mTORC1 activity has been studied in HD and may have a critical role in disease pathogenesis. mHTT aggregates sequester mTOR, and inducing autophagy with rapamycin limits aggregates and improves behavioral phenotypes, particularly when administered before symptom onset (Ravikumar et al., 2004). Rapamycin may specifically benefit skeletal muscle in R6/2 mice, a tissue with increased mTORC1 activity (She et al., 2011). However, in other work, mTORC1 activity was notably reduced in HD rodent and human brain, and restoring mTORC1 activity alleviated neuropathology and motor deficits in mouse models of HD (Lee et al., 2015). Given mTORC1's importance in heart size and stress adaptation, mTORC1 activity may be similarly compromised in the HD heart, causing phenotypic changes that predispose the development of cardiomyopathy.

RESULTS

Decreased Mass in HD Mouse Hearts Results from Limited Growth

We used two HD mouse models to study the effect of HD on the heart. The transgenic N171-82Q mouse expresses the N-terminal 171-amino acid fragment of HTT with an expanded 82 polyglutamine region and causes robust neurological and metabolic phenotypes (Schilling et al., 1999). The zQ175 knockin mouse expresses a human-mouse chimeric mHTT with a 188-residue polyglutamine tract knocked into one of the two endogenous *huntingtin* alleles (only heterozygotes were used for these studies). zQ175 mice have a slower disease course than the N171-82Q model (Menalled et al., 2012). Importantly, both models express mHTT in the heart.

Heart function in HD mice was assessed by transthoracic echocardiography. N171-82Q mice (18-week-old; end-stage disease) had decreased left ventricular end diastolic (LVEDV) and systolic volumes (LVESV), and decreased heart rate (HR) relative to wild-type (WT) littermates, with a corresponding reduction in cardiac output (CO) (Figure 1A). However, ejection fraction (EF) in transgenic animals was moderately elevated relative to WT (Figure 1A), suggesting HD mice have reduced cardiac mass than their WT littermates but maintain intact ventricular function at end-stage disease.

Excised hearts from N171-82Q mice at end-stage disease were visibly smaller than their WT littermates but with no apparent morphologic differences such as ventricular dilation (Figure 1B). When tracked temporally, decreased heart mass in HD relative to WT mice became apparent at 10 weeks (early-stage disease) and continued to manifest throughout the lifespan (Figure 1C). The growth curves show that the differences between HD and WT heart masses result from failure to gain mass around the time of symptom onset, a trend consistent with the reported pattern of body mass changes in HD patient populations (Hamilton et al., 2004). Mass differences were maintained after normalizing heart mass to tibia length, with the decreased ratio in HD mice indicating uninhibited skeletal growth and ruling out lack of growth factors as an explanation for heart mass differences (Figure 1C). There was no difference in tibia length between WT and N171-82Q animals (Figure S1A). The heart mass-to-body mass ratio does not differ between WT and N171-82Q animals until 14 weeks (mid-stage disease), at which time it is larger in N171-82Q animals relative to WT, suggesting that the heart mass does not change proportionally with the rest of the body (Figure S1B). Indeed, comparing heart mass and body mass in N171-82Q mice over lifespan

shows relatively constant heart mass while body mass fluctuates (Figure S1C). In zQ175 animals at 12 months of age (post symptomatic), heart mass and heart mass-to-tibia length are both decreased, similar to and confirming findings in N171-82Q animals (Figure 1D). There were no differences in either tibia length or heart mass to body mass ratio in zQ175 animals (Figures S1D and S1E).

To further address heart mass differences, we used wheat germ agglutinin staining to identify cardiomyocyte borders and measured cross-sectional area. There was no difference in mean cross-sectional area in 6-week-old N171-82Q mice relative to WT littermates, but 14-week-old N171-82Q mice and 12-month-old zQ175 mice had decreased myocardial cross-sectional area relative to WT (Figure 2A). We next used Masson's trichrome stain to identify fibrosis resulting from cardiomyocyte death but found no evidence of fibrosis in HD hearts from N171-82Q mice at 6 weeks (pre-symptomatic) or 14 weeks of age, or in zQ175 animals at 12 months of age (Figure 2B). Cardiomyocytes isolated from 14-week-old N171-82Q hearts (mid-stage disease) had smaller surface area than age-matched WT cardiomyocytes (Figure 2C). TUNEL stain of 18-week N171-82Q hearts showed no evidence of apoptosis (Figure S1F). Together, these data denote limited cardiomyocyte growth in HD models accounting for mass differences, not cardiomyocyte loss.

Gene signatures associated with heart failure have been detected in HD mouse model hearts (Mielcarek et al., 2014b; Schroeder et al., 2016). Typically, these genes sense stress and limit maladaptive changes. Atrial natriuretic peptide (*Anp*) and brain natriuretic peptide (*Bnp*) are hormones expressed in the ventricles and reduce central venous pressure in response to excessive cardiomyocyte stretching (Kinnunen et al., 1993). *Anp* and *Bnp* expression were both decreased at 14 and 18 weeks in N171-82Q animals—opposite the expected findings in heart failure—and BNP expression was also decreased at 6 weeks in N171-82Q mice (Figures S1G and S1H). No differences were observed between zQ175 and WT hearts at 12 months. Physiologically significant expression changes in other genes associated with heart failure were not detected in either model (data not shown), confirming functional analyses and suggesting that these mice do not experience heart failure as a result of cardiac mHTT expression.

mTORC1 Activity Is Decreased in HD Mice Hearts

We assessed mTORC1 activity in HD mouse model hearts by measuring phosphorylation of the mTORC1 targets ribosomal protein S6 (P-S6) and initiation factor 4E binding protein 1 (P-4EBP1). Both P-S6 and P-4EBP1 levels were decreased relative to WT in N171-82Q hearts beginning at 6 weeks of age and continuing throughout all disease stages; similar decreases in P-S6 and P-4EBP1 were also present in 12-month zQ175 mouse hearts (Figure 3A). Immunohistochemical analysis of P-S6 in N171-82Q hearts at 6 and 14 weeks and zQ175 hearts at 12 months showed P-S6 localizing at what appear to be the intercalated discs between adjacent cardiomyocytes. Consistent with the western blot data, P-S6 stains more intensely in WT hearts than HD hearts (Figure 3B). As a whole, these data indicate decreased mTORC1 activity in HD hearts.

miRNA-Mediated Knock Down of mHTT Restores Cardiac mTORC1 Activity

If mHTT expression causes mTORC1 dysregulation, reducing mHTT levels should ameliorate that phenotype. Cardiac-specific gene transduction was achieved using a previously undescribed cardiotropic variant of AAV2 (CT.AAV) that exhibits robust preference for cardiomyocytes (Figure 4A). 5-week-old, presymptomatic N171-82Q mice were treated with CT.AAV to deliver a miRNA targeting HTT (mi2.1), a non-targeting control (miCTRL), or formulation buffer (FB). Treatment effects were assessed when mice were 16 weeks of age, corresponding to late-stage disease. In mice treated with CT.AAV.mi2.1, qPCR and WB indicated Ĩ40% decrease in cardiac HTT mRNA (Figure 4B) and 35% decrease in cardiac HTT protein (Figures 4C and 4D), respectively, with P-S6 and P-4EBP1 levels robustly increased relative to controls (Figures 4E–4G). These results collectively suggest that cardiac mHTT expression is necessary for mTORC1 inhibition.

HD Mice Have Blunted Adaptation to Cardiac Stress

The heart adapts to pathologic stressors (e.g., hypertension, valve stenosis or insufficiencies, myocardial infarction) and maintains cardiac output by hypertrophy, a process mediated by mTORC1. Heart hypertrophy can eventually become maladaptive, but in its early stages it permits continued function and survival. We tested adaptation to cardiac stress in HD using the well-characterized pharmacological model isoprenaline (ISO), a nonspecific β-adrenergic agonist used clinically to increase heart rate, contractility, and conduction speed (Wang et al., 2016). Infusions were started at 12 weeks of age and continued for 14 days; at this age, N171-82Q animals are symptomatic but are not yet experiencing terminal disease. With stress, N171-82Q mice experienced 50% mortality over the course of the study compared to 15% mortality in N171-82Q mice treated with saline and 0% mortality in WT mice treated with either ISO or saline (Figure 5A). Similarly stressed 18-month-old zQ175 mice experienced 83% mortality compared to 25% mortality in stressed WT littermates and 0% in saline-treated mice of either genotype (Figure 5B), confirming that HD mice have increased susceptibility to chronic stress and implicating age as an aggravating factor.

The *in vivo* cardiac stress response in HD mice was studied by transthoracic echocardiography. Imaging in HD and WT mice was performed at baseline, prior to ISO (or treatment control) delivery, and again 5 and 12 days later, and the temporal change from baseline assessed. ISO-stressed N171-82Q mice had increased fractional shortening (FS), HR, CO, and EF at trial days 5 and 12 relative to baseline, but there was no significant change in left ventricular mass (LV mass) (Figures 5C and S2A). Conversely, ISO-stressed WT animals showed significant LV mass increase from baseline at trial days 5 and 12, with unchanged or no significant changes in FS, HR, CO, and EF at both time points (Figures 5C and S2A). ISO did not induce measurable changes in LVEDV or LVESV in either genotype (Figure S2A). These results demonstrate that WT hearts employ a hypertrophic adaptation in response to chronic ISO stress, whereas HD hearts undergo sustained increase of heart rate and contractility but do not hypertrophy.

To confirm limited hypertrophy as measured by echocardiography we measured both gross heart mass and cardiomyocyte cross-sectional area post necropsy and tissue sectioning. Average heart mass/tibia length increased by 35.3% in WT animals treated with ISO relative

to saline-treated WT controls and by a blunted 18.7% in HD animals treated with ISO relative to saline-treated HD controls (Figure S2B; note that this data reflect only the surviving mice at trial endpoint). Additionally, ISO induced robust cardiomyocyte cross-sectional area increase in WT mice relative to saline-treated controls, but it failed to increase the cross-sectional area of HD cardiomyocytes (Figure 5D). Heart sections stained with Masson's Trichrome (Figure 5E) or picrosirius red (Figure S2C) showed that both WT and HD mice treated with ISO had increased fibrosis relative to saline-treated animals, but the extent of fibrosis was significantly greater in HD hearts. Cardiomyocyte apoptosis in stressed hearts was assessed by TUNEL stain, which was negative for all treatment groups (data not shown). We therefore examined transcripts encoding the apoptosis activator *Bax* and the anti-apoptotic factor *Bcl2. Bax* was moderately but significantly elevated in ISO-treated HD and WT hearts relative to saline controls and *Bcl2* expression was decreased in stressed hearts (Figure S2D). Taken together, these results demonstrate that HD animals have impaired hypertrophic compensation to cardiac stress with significantly elevated fibrosis.

Decompensated heart failure occurs when pathogenic or compensatory processes become maladaptive and impair cardiac function, which leads to increased pulmonary pressure and fluid accumulation in the lungs. The wet/dry lung mass ratio can therefore be used as an indicator of heart failure. In N171-82Q and WT mice treated with ISO or saline for 14 days we observed no differences in the wet/dry lung mass ratio, suggesting that the animals surviving to this time point are not experiencing decompensated heart failure (Figure S2E). However, only tissue from animals that survived to the end of the trial were included in the analysis due to rapid, confounding, post-mortem lung changes. Additionally, in stressed hearts from both WT and HD animals that survived to trial endpoint, mTORC1 activity was increased as measured by P-S6/S6 levels, with significant variability in HD hearts (Figure S2F). P-4EBP1/4EBP1 levels were not different among treatment groups, with a similar large variance observed in surviving stressed HD mice hearts (Figure 5E). These observations suggest that partially overcoming the inherent cardiac mTORC1 dysregulation in HD mice may be associated with survival to trial endpoint.

mTORC1 Activation in HD Hearts Restores the Adaptive Cardiac Stress Response

We studied the relevance of mTORC1 inhibition in the HD cardiac stress response by selectively activating cardiac mTORC1 in N171-82Q hearts. CT.AAV was used to express a constitutively active variant of Rheb (Rheb-S16H, or simply caRheb) or GFP in HD mice hearts (Yan et al., 2006). Successful caRheb transduction was confirmed by western blot (Figure S3A). Two weeks after vector delivery, heart stress was induced by ISO or saline infusion as before (Figure 6A). As expected, HD mice transduced with CT.AAV.GFP and treated with ISO (GFP-ISO) experienced increased mortality relative to saline-treated mice transduced with either CT.AAV.GFP or CT.AAV.caRheb (GFP-saline and caRheb-saline, respectively) (Figure 6B). In contrast, HD mice transduced with CT.AAV.caRheb and treated with isoprenaline (caRheb-ISO), displayed significantly less mortality over the course of the study (Figure 6B). Thus, cardiac caRheb expression ameliorates sensitivity to ISO stress in HD mice.

On transthoracic echocardiogram, the GFP-ISO group displayed increased FS, HR, and EF from baseline without an increase in LV mass at trial days 5 and 12 (Figures 6C and S3B), similar to the observations made in stressed non-AAV-treated N171-82Q hearts (Figures 5C and S2A). Conversely, the caRheb-ISO group responded to stress with an increase in LV size from pretreatment levels, with no changes in FS, HR, or EF from pretreatment levels at either time point (Figures 6C and S3B), approximating the WT response to chronic ISO (Figures 5C and S2A). There were no measurable changes in LVEDV, LVESV, and CO for either vector (Figure S3B). These measurements collectively imply that caRheb transduction restores the functional stress response in HD hearts.

The effects of caRheb transduction on the cardiac stress response in HD mice were further studied by examining heart mass/tibia length. There were no differences observed between GFP-saline, GFP-ISO, and caRheb-saline groups. However, caRheb-ISO-treated HD mice showed a 27.5% increase in heart mass/tibia length (Figure S3C). Analysis of cardiomyocyte cross-sectional area in the HD mice showed no difference between the GFP-saline and GFP-ISO groups (Figure 6D). In caRheb-treated HD mice, the saline group had moderately increased cardiomyocyte cross-sectional area relative to the GFP- saline group. Notably, caRheb-ISO-treated mice showed robust cross-sectional area increase relative to all other groups, representing restored hypertrophic adaptation (Figure 6D). The impact of caRheb on restoration of proper compensation to chronic stress was further apparent in analyses of fibrosis by Masson's trichrome (Figure 6E) and picrosirius red stains (Figure S3D): extensive fibrosis was present in hearts from the GFP-ISO-treated HD mice, whereas fibrosis in hearts from the caRheb-ISO group was almost entirely absent (Figure 6E). TUNEL stain to detect apoptotic nuclei was negative in all treatment groups (data not shown), but qPCR analysis of apoptotic factors showed moderately but significantly increased *Bax* expression in the caRheb-ISO group only, and no significant changes in *Bcl2* expression (Figure S3E). Together, these results show that caRheb expression in HD hearts allows cardiomyocyte hypertrophy and prevents deposition of fibrotic tissue in response to stress.

Similar to before, wet/dry lung mass ratios of mice surviving to trial endpoint were not different between groups, suggesting that the mice included in the assay were not experiencing decompensated heart failure at the time of observation (Figure S3F). Additionally, as before, mTORC1 activity in hearts of surviving animals was increased with ISO treatment (Figure S3G). While P-S6/S6 levels in caRheb-transduced mice groups trended higher than their respective GFP-transduced mice groups, they did not achieve statistical significance due in part to large variance in surviving GFP-ISO samples. Thus, the ability to overcome the dysregulated cardiac mTORC1 activity in HD hearts, through endogenous or exogenous means, is associated with survival in response to stress.

Molecular Mechanism of Cardiac Dysregulation in HD

We analyzed upstream members in the mTORC1 pathway to determine the molecular basis for mTORC1 dysregulation in HD mice (Figure 7A). We first asked if decreased cardiac mTORC1 activity is due to decreased axis activation. IGF-I, a PI3K-Akt-mTORC1 pathway activator, was unexpectedly increased in 6-week-old N171-82Q mice serum relative to WT, but normalized by 14 weeks (Figure 7B). Serum IGF-I was unchanged in presymptomatic 6-

month zQ175 mice and slightly decreased in 12-month zQ175. Expression of IGF-I receptor RNA, *Igf1r*, was equal between N171-82Q and WT hearts at 6 weeks and between zQ175 and WT hearts at 12 months, but increased in N171-82Q hearts relative to WT at later time points (Figure 7C). Phosphorylation of Erk, a downstream target of IGF-I signaling independent of the mTORC1 pathway, did not differ between HD and WT at any time point in N171-82Q mice or in 12-month-old zQ175 mice (Figure S4A). Insulin, another mTORC1 pathway activator, was decreased in 14-week N171-82Q serum (Figure S4B). Note that N171-82Q mice at this stage experience altered feeding patterns (Figure S4C) that could affect insulin secretion.

Next, we examined intracellular pathways that regulate mTORC1. Modest differences existed in phosphatase and tensin homolog (*Pten*) mRNA expression at 6 weeks, an early negative regulator of the mTORC1 pathway, but the changes were so slight that functional significance is unlikely. No differences existed at later time points or in 12-month zQ175 animals (Figure 7D). Growth factor signals are transmitted intracellularly to mTORC1 via the kinases PDK1 and Akt. Phosphorylated Akt (P-Akt, indicative of PDK1 activity) and phosphorylated mTOR (P-mTOR, indicative of Akt activity) were both significantly decreased in 6-week N171-82Q hearts relative to WT and in 12-month zQ175 hearts (Figures 7E–7G). However, P-Akt and P-mTOR levels were not different between HD and WT at post-symptomatic time points in N171-82Q mice. The early decrease, followed by normalization, suggests that the diminished PDK1 activity impairs mTORC1 activation at presymptomatic and early disease stages, but not later stages.

We next examined phosphorylation of AMPKa, which occurs in response to energy deficits within cells and permits AMP kinase (AMPK) to inhibit mTORC1. P-AMPKα levels were not different at any time point in N171-82Q mice or in 12-month zQ175 mice relative to WT mice (Figure 7E and H), suggesting that the noted cardiac mTORC1 dysregulation does not result from systemic energy imbalance.

The forkhead box protein O (FoxO) transcription factor family coordinates expression of genes that generally oppose the downstream functions of mTORC1 (Puthanveetil et al., 2013). Gene targets of the FoxO family include gene products that contribute to muscle atrophy, as well as *Bnip3*, an inhibitor of mTORC1 (Li et al., 2007; Lin et al., 2014). Previous reports have associated HD with increased FoxO3 expression in the brain (Kannike et al., 2014). *FoxO1* expression was elevated relative to WT in both in N171-82Q hearts starting at 6 weeks and in zQ175 mouse hearts at 12 months (Figure S5A). *FoxO3* expression was elevated only in N171-82Q hearts at 14 and 18 weeks (Figure S5B). Expression of *Bnip3* in HD hearts did not differ from WT at any time point in N171-82Q mice or in zQ175 hearts (Figure S5C). These data suggest that the FoxO pathway is not impairing mTORC1 activity in the heart.

Activation of mTORC1 relies both on signaling cascades and on proper localization of the various subunits of the complex to internal membranes. As none of the probable signaling pathways could explain the mTORC1 dysregulation in either model, we examined subcellular localization of mTORC1 components. Membrane extraction on N171-82Q mouse hearts at 16 weeks of age showed that Rheb, the activating subunit of mTORC1, was

increased in the cytoplasmic fraction and decreased in the membrane fraction (Figure 7I). Rheb localization did not differ between N171-82Q and WT hearts at 6 weeks of age (Figure S6A), consistent with previous results showing differences in mTORC1 dysregulation between presymptomatic and symptomatic HD mice. Altering Rheb's ability to properly localize has previously been shown to inhibit mTORC1 activity, and thus Rheb mislocalization may underlie the impairment of mTORC1 in symptomatic HD mice hearts. Additionally, caRheb overexpression could overcome the deficiency imparted by endogenous mislocalization.

DISCUSSION

HD is a neurodegenerative disease, but ubiquitous mHTT expression has adverse effects outside of the CNS. Indeed, epidemiological data indicate that the heart plays a central role as a major component of mortality in HD patients (Lanska et al., 1988a, 1988b; Sørensen and Fenger, 1992). Here, we characterized the cardiac phenotype resulting from mHTT expression in two HD mouse models and found that HD hearts have decreased size but are not functionally impaired in the absence of cardiac stress. Additionally, cardiac mTORC1 is dys-regulated in HD murine models, and the knock down of mHTT restores mTORC1 activity. The physiological relevance of the mTORC1 dysregulation in the HD heart is that it prevents proper adaptation to hemodynamic stress and sensitizes the heart to pathologic conditions; under cardiovascular stress conditions HD mice exhibit increased mortality, blunted heart hypertrophy, and extensive myocardial fibrosis. Importantly, these abnormalities were abrogated following activation of cardiac mTORC1, implicating decreased mTORC1 activity as central to development of heart disease with stress in HD mice. In the transgenic and KI models studied, chronic mTORC1 dysregulation in HD is not explained by inhibitory upstream signaling. However, Rheb's subcellular localization is altered, which can negatively impact mTORC1 activity (Basso et al., 2005; Buerger et al., 2006; Castro et al., 2003). Cumulatively our data suggest that mHTT's impact on mTORC1 impairs the ability of cardiomyocytes to respond to stressors, which may underlie the etiology of heart disease-induced death in HD patients.

A recent review on peripheral HD phenotypes presents data that identifies *HTT* mRNA expression within the heart but suggests no HTT protein expression (Carroll et al., 2015). This conclusion is based on data from the Human Protein Atlas, which uses a qualitative IHC approach and assigns a score of zero if at least one out of two antibodies fails to produce a signal; thus, lack of expression and uncertain assay results are considered equivalent (Uhlén et al., 2015). Fortunately, multiple high-throughput proteomics analyses using mass spectrometry have identified HTT protein within the heart, consistent with the RNA sequencing (RNA-seq) data (Wang et al., 2012; Wilhelm et al., 2014).

Functional analyses in cardiac stress experiments showed that HD hearts experience increased rate and contractility in response to chronic isoprenaline, whereas WT hearts (and HD hearts transduced with CT.AAV.caRheb) respond by hypertrophy. Heart hypertrophy is frequently considered a pathologic process, and indeed, substantial proliferation and reorganization of cardiac myofibrils can decrease efficiency and conduction, restrict blood supply, and lead to heart failure (Beache et al., 2001; Norton et al., 2002). However, before

the compensatory processes become pathologic in and of themselves, hypertrophy decreases the amount of work the heart must exert in response to a stressor (according to the Laplace law) and can therefore be considered an indicator of an underlying pathology before it becomes maladaptive (Cotecchia et al., 2015). Consequently, without hypertrophy, the HD hearts' response to stress requires more work—therefore energy—than their WT littermates. This chronic, high-energy response, coupled with functional mitochondrial abnormalities (Toczek et al., 2016), may make HD cardiomyocytes more susceptible to exhaustion and might explain the increased mortality and fibrosis observed in stressed HD animals. While characterizing the specific pathophysiology of stressed HD hearts is outside the scope of these studies, future efforts to understand mortality in stressed HD mouse hearts could employ *ex vivo* bioenergetics to confirm unbalanced ATP metabolism, electrocardiographic telemetry to determine if fatal arrhythmias contribute to death, and invasive hemodynamics to assess pressure, resistance, and flow changes upon chronic stress.

Similar to studies in brain (Lee et al., 2015), cardiac mTORC1 activity was dysregulated before motor symptom onset, suggesting that molecular pathogenesis associated with mHTT expression begins early and contributes to the notable, limited heart growth. Interestingly, the cause of mTORC1 dysregulation results from distinct etiologies based on disease stage. Pre-symptomatic mTORC1 dysregulation is associated with decreased upstream activation, whereas upstream signaling activity is normal in post-symptomatic HD mice. The later-stage mTORC1 dysregulation, even when upstream signals are normal, is likely due to Rheb mislocalization. Rheb is post-translationally modified with a farnesyl group that targets it to the cellular endomembranes in the ER, Golgi, mitochondria, and late endosomes/lysosomes (Buerger et al., 2006; Sancak et al., 2008). Inhibiting this process induces Rheb mislocalization and impairs mTORC1 activity (Basso et al., 2005; Castro et al., 2003). Farnesyl is a metabolic precursor product in the cholesterol biosynthesis pathway, a process impaired in HD (Leoni and Caccia, 2015), and lysosomal cholesterol stores are essential for proper mTORC1 localization and activation (Castellano et al., 2017). While it is still unknown if Rheb in late-stage HD hearts mislocalizes due to lack of farnesylation or through another mechanism, it is possible that aberrant cholesterol metabolism in HD may contribute to the decreased mTORC1 activity observed in both the heart and the brain.

With CNS-directed HTT-lowering therapy in HD patients progressing in clinical trials (Ionis Pharmaceuticals, 2017), there is a pressing need to identify the consequences of mHTT expression in the heart and other peripheral organs that may be unmasked with amelioration of CNS deficits. Future studies on human HD heart tissues, which at the present time are not routinely collected, will help illuminate the temporal nature of reduced cardiac mass in HD patients, and if mTORC1 plays as central a role in the phenotype. Our data are also relevant to those contemplating the use of mTORC1 inhibitors in HD, raising cardiac issues as a possible contraindication. Finally, this work demonstrates the pressing need within the field for expanded tissue banks and clinical studies to adequately understand the heart and other peripheral phenotypes in HD, as well as other neurodegenerative diseases.

EXPERIMENTAL PROCEDURES

Study Approval

All animal protocols were conducted in accordance with the NIH *Guide for the Care and Use of Laboratory Animals* and were approved by the Animal Care and Use Committee at either the University of Iowa or The Children's Hospital of Philadelphia.

Animals

N171-82Q and zQ175 HD murine model lines were obtained from Jackson Laboratories and maintained on a B6C3F1/J (N171-82Q) or C56B6/J (zQ175) background. Mice were genotyped using primers specific for human HTT, and age-matched WT littermates were used as controls for all experiments. All studies were performed with male mice exclusively. Animals were housed in enriched, temperature-controlled environments with a 12-hr light/dark cycle. Food and water were provided *ad libitum*.

Echocardiography

Mice were anesthetized with 2.5% isoflurane and positioned on a heated stage with electrocardiogram (EKG) measurement. Transthoracic echocardiograms were recorded using an MS-400 30 MHz probe connected to a Vevo 2100 or 3100 imager with cardiovascular measurement package. (Fujifilm VisualSonics). Images were acquired and dimensions measured by an experienced operator blinded to mouse genotype. Cardiac output was calculated as the difference between left ventricular end diastolic and systolic volumes multiplied by the heart rate.

Histology Analyses

For wheat germ agglutinin staining, images were taken throughout the posterior wall to encompass all transversely sectioned cells. ImageJ was used to overlay a grid on each image to randomly select approximately 50 cells/image and cross-sectional area was measured for each selected cell. At least 200 cells were measured per heart. For picrosirius red-stained sections, low-power images were taken using both a standard bright field filter and a polarizing filter. At least 9 images were collected per heart, capturing a large section of the left ventricle. Large vessels were avoided because of their high collagen content. ImageJ was used to threshold and measure area of each image, and percent of total area occupied by fibrotic tissue was used for analyses.

Western Blot Analysis

Densitometrywas performed using NIHImageJ software. Densities of bands detected by phospho-antibodies were normalized to densities of bands detected by phospho-independent antibodies in same lane. Phospho-independent antibody densities were normalized to a-tubulin or Na/K-ATPase band in same lane.

IGF-I and Insulin Measurements

Mouse blood was collected retro-orbitally using microcapillary tubes. Blood was allowed to clot for 15 min at room temperature, and serum was isolated by centrifugation. Serum IGF-I

and insulin was detected by colorimetric ELISA (IGF-I, Thermo Fisher Scientific; insulin, Crystal Chem).

qPCR Analyses

Relative gene expression was determined using the ΔΔCT method, normalizing to TATA-binding protein (*Tbp*) or *Gapdh*. Standard curves to determine copies/mg RNA were prepared using plasmids containing the gene of interest.

Plasmids and AAVs

Cardiotropic AAV (termed CT.AAV) was developed by inserting a nine-residue peptide sequence identified by phage panning into the *cap* gene of AAV2. Genes of interest were cloned into a standard AAV2 expression cassette. MicroRNA systems (mi2.1, miCTRL) were previously developed by the lab (Harper et al., 2005) and were driven by a U6 promoter. Rheb-S16H (constitu-tively active Rheb, caRheb) plasmids were developed as previously described and were driven by a CAG promoter (CMV enhancer linked to a β-actin promoter) (Lee et al., 2015). All AAVs were made by the Research Vector Core at The Children's Hospital of Philadelphia. Titers (measured in viral genomes/mL) were determined by qPCR.

Cardiac Stress Induction

Isoprenaline (ISO, Sigma) was dissolved in sterile PBS and administered by continuous infusion using implantable mini-osmotic pumps (Alzet) at a dose of 30 mg/kg body mass/day. Pumps were filled and primed in a sterile environment and were inserted into the dorsal subcutaneous space caudal to the scapulae.

Statistics

Data were analyzed with Student's t test or one-way ANOVA with Tukey's post hoc analysis to assess differences in experimental groups. All statistical tests were two-sided. Normality was determined graphically and by Shapiro-Wilk test. Survival curves were analyzed by Mantel-Cox (log-rank) test. All analyses were performed using GraphPad Prism version 7.03 or R version 3.2.1. Data are expressed as mean ± SEM, and for all analyses, $p \leq 0.05$ was considered significant.

Supplementary Material

Refer to Web version on PubMed Central for supplementary material.

Acknowledgments

The authors gratefully acknowledge Dr. Olha Koval (University of Iowa) for performing primary adult cardiomyocyte isolation, The Children's Hospital of Philadelphia Research Vector Core for preparation of AAV vectors, The Children's Hospital of Philadelphia Small Animal Imaging Facility for hosting the ultrasound instrument, and The Children's Hospital of Philadelphia Pathology Core for paraffin processing and embedding of fixed tissue. This work was supported by the NIH (NS084475 and NS076631 to B.L.D.). D.D.C. is supported by NIH T32 HL007954. J.H.L. was supported by NIH T32 HL007638.

References

Abildtrup M, Shattock M. Cardiac dysautonomia in Huntington's disease. J Huntingtons Dis. 2013; 2:251–261. [PubMed: 25062674]

Bär KJ, Boettger MK, Andrich J, Epplen JT, Fischer F, Cordes J, Koschke M, Agelink MW. Cardiovagal modulation upon postural change is altered in Huntington's disease. Eur J Neurol. 2008; 15:869–871. [PubMed: 18484985]

Basso AD, Mirza A, Liu G, Long BJ, Bishop WR, Kirschmeier P. The farnesyl transferase inhibitor (FTI) SCH66336 (lonafarnib) inhibits Rheb farnesylation and mTOR signaling. Role in FTI enhancement of taxane and tamoxifen anti-tumor activity. J Biol Chem. 2005; 280:31101–31108. [PubMed: 16006564]

Beache GM, Herzka DA, Boxerman JL, Post WS, Gupta SN, Faranesh AZ, Solaiyappan M, Bottomley PA, Weiss JL, Shapiro EP, Hill MN. Attenuated myocardial vasodilator response in patients with hypertensive hypertrophy revealed by oxygenation-dependent magnetic resonance imaging. Circulation. 2001; 104:1214–1217. [PubMed: 11551869]

Bellosta Diago E, Pérez-Pérez J, Santos Lasaosa S, Viloria Alebesque A, Martínez-Horta S, Kulisevsky J, López Del Val J. Neurocardio-vascular pathology in Premanifest and Early Stage Huntington's Disease. Eur J Neurol Published online March. 2018; 14:2018. https://doi.org/10.1111/ene.13630.

Boluyt MO, Zheng JS, Younes A, Long X, O'Neill L, Silverman H, Lakatta EG, Crow MT. Rapamycin inhibits alpha 1-adrenergic receptor-stimulated cardiac myocyte hypertrophy but not activation of hypertrophy-associated genes. Evidence for involvement of p70 S6 kinase Circ Res. 1997; 81:176–186. [PubMed: 9242178]

Boudreau RL, McBride JL, Martins I, Shen S, Xing Y, Carter BJ, Davidson BL. Nonallele-specific silencing of mutant and wild-type huntingtin demonstrates therapeutic efficacy in Huntington's disease mice. Mol Ther. 2009; 17:1053–1063. [PubMed: 19240687]

Buerger C, DeVries B, Stambolic V. Localization of Rheb to the endomembrane is critical for its signaling function. Biochem Biophys Res Commun. 2006; 344:869–880. [PubMed: 16631613]

Carroll JB, Bates GP, Steffan J, Saft C, Tabrizi SJ. Treating the whole body in Huntington's disease. Lancet Neurol. 2015; 14:1135–1142. [PubMed: 26466780]

Castellano BM, Thelen AM, Moldavski O, Feltes M, van der Welle RE, Mydock-McGrane L, Jiang X, van Eijkeren RJ, Davis OB, Louie SM, et al. Lysosomal cholesterol activates mTORC1 via an SLC38A9-Niemann-Pick C1 signaling complex. Science. 2017; 355:1306–1311. [PubMed: 28336668]

Castro AF, Rebhun JF, Clark GJ, Quilliam LA. Rheb binds tuberous sclerosis complex 2 (TSC2) and promotes S6 kinase activation in a rapamycin- and farnesylation-dependent manner. J Biol Chem. 2003; 278:32493–32496. [PubMed: 12842888]

CDC. National Health and Nutrition Examination Survey: NHANES III (1988–1994). 1994. https://wwwn.cdc.gov/nchs/nhanes/nhanes3/default.aspx

Chaturvedi RK, Calingasan NY, Yang L, Hennessey T, Johri A, Beal MF. Impairment of PGC-1alpha expression, neuropathology and hepatic steatosis in a transgenic mouse model of Huntington's disease following chronic energy deprivation. Hum Mol Genet. 2010; 19:3190–3205. [PubMed: 20529956]

Cotecchia S, Del Vescovo CD, Colella M, Caso S, Diviani D. The alpha1-adrenergic receptors in cardiac hypertrophy: signaling mechanisms and functional implications. Cell Signal. 2015; 27:1984–1993. [PubMed: 26169957]

Cutler TS, Park S, Loh DH, Jordan MC, Yokota T, Roos KP, Ghiani CA, Colwell CS. Neurocardiovascular deficits in the Q175 mouse model of Huntington's disease. Physiol Rep. 2017; 5:e13289. [PubMed: 28576852]

Goorden SM, Hoogeveen-Westerveld M, Cheng C, van Woerden GM, Mozaffari M, Post L, Duckers HJ, Nellist M, Elgersma Y. Rheb is essential for murine development. Mol Cell Biol. 2011; 31:1672–1678. [PubMed: 21321084]

Hamilton JM, Wolfson T, Peavy GM, Jacobson MW, Corey-Bloom J, Huntington Study Group. Rate and correlates of weight change in Huntington's disease. J Neurol Neurosurg Psychiatry. 2004; 75:209–212. [PubMed: 14742590]

Harper SQ, Staber PD, He X, Eliason SL, Martins IH, Mao Q, Yang L, Kotin RM, Paulson HL, Davidson BL. RNA interference improves motor and neuropathological abnormalities in a Huntington's disease mouse model. Proc Natl Acad Sci USA. 2005; 102:5820–5825. [PubMed: 15811941]

Ikeda M, Ide T, Fujino T, Matsuo Y, Arai S, Saku K, Kakino T, Oga Y, Nishizaki A, Sunagawa K. The Akt-mTOR axis is a pivotal regulator of eccentric hypertrophy during volume overload. Sci Rep. 2015; 5:15881. [PubMed: 26515499]

Ionis Pharmaceuticals. Ionis Pharmaceuticals Licenses IONIS-HTTRx to Partner Following Successful Phase 1/2a Study in Patients with Huntington's Disease. PRNewswire. 2017. December 11, 2017. http://ir.ionispharma.com/news-releases/news-release-details/ionis-pharmaceuticals-licenses-ionis-htt-rx-partner-following

Kannike K, Sepp M, Zuccato C, Cattaneo E, Timmusk T. Forkhead transcription factor FOXO3a levels are increased in Huntington disease because of overactivated positive autofeedback loop. J Biol Chem. 2014; 289:32845–32857. [PubMed: 25271153]

Kinnunen P, Vuolteenaho O, Ruskoaho H. Mechanisms of atrial and brain natriuretic peptide release from rat ventricular myocardium: effect of stretching. Endocrinology. 1993; 132:1961–1970. [PubMed: 8477647]

Kobal J, Meglic B, Mesec A, Peterlin B. Early sympathetic hyperactivity in Huntington's disease. Eur J Neurol. 2004; 11:842–848. [PubMed: 15667417]

Lanska DJ, Lanska MJ, Lavine L, Schoenberg BS. Conditions associated with Huntington's disease at death. A case-control study Arch Neurol. 1988a; 45:878–880. [PubMed: 2969233]

Lanska DJ, Lavine L, Lanska MJ, Schoenberg BS. Huntington's disease mortality in the United States. Neurology. 1988b; 38:769–772. [PubMed: 2966305]

Laplante M, Sabatini DM. mTOR signaling in growth control and disease. Cell. 2012; 149:274–293. [PubMed: 22500797]

Lee JH, Tecedor L, Chen YH, Monteys AM, Sowada MJ, Thompson LM, Davidson BL. Reinstating aberrant mTORC1 activity in Huntington's disease mice improves disease phenotypes. Neuron. 2015; 85:303–315. [PubMed: 25556834]

Leoni V, Caccia C. The impairment of cholesterol metabolism in Huntington disease. Biochim Biophys Acta. 2015; 1851:1095–1105. [PubMed: 25596342]

Li SH, Schilling G, Young WS 3rd, Li XJ, Margolis RL, Stine OC, Wagster MV, Abbott MH, Franz ML, Ranen NG, et al. Huntington's disease gene (IT15) is widely expressed in human and rat tissues. Neuron. 1993; 11:985–993. [PubMed: 8240819]

Li Y, Wang Y, Kim E, Beemiller P, Wang CY, Swanson J, You M, Guan KL. Bnip3 mediates the hypoxia-induced inhibition on mammalian target of rapamycin by interacting with Rheb. J Biol Chem. 2007; 282:35803–35813. [PubMed: 17928295]

Lin A, Yao J, Zhuang L, Wang D, Han J, Lam EW, Gan B. The FoxO-BNIP3 axis exerts a unique regulation of mTORC1 and cell survival under energy stress. Oncogene. 2014; 33:3183–3194. [PubMed: 23851496]

McBride JL, Pitzer MR, Boudreau RL, Dufour B, Hobbs T, Ojeda SR, Davidson BL. Preclinical safety of RNAi-mediated HTT suppression in the rhesus macaque as a potential therapy for Huntington's disease. Mol Ther. 2011; 19:2152–2162. [PubMed: 22031240]

Melkani GC, Trujillo AS, Ramos R, Bodmer R, Bernstein SI, Ocorr K. Huntington's disease induced cardiac amyloidosis is reversed by modulating protein folding and oxidative stress pathways in the Drosophila heart. PLoS Genet. 2013; 9:e1004024. [PubMed: 24367279]

Menalled LB, Kudwa AE, Miller S, Fitzpatrick J, Watson-Johnson J, Keating N, Ruiz M, Mushlin R, Alosio W, McConnell K, et al. Comprehensive behavioral and molecular characterization of a new knock-in mouse model of Huntington's disease: zQ175. PLoS ONE. 2012; 7:e49838. [PubMed: 23284626]

Mielcarek M, Bondulich MK, Inuabasi L, Franklin SA, Muller T, Bates GP. The Huntington's disease-related cardiomyopathy prevents a hypertrophic response in the R6/2 mouse model. PLoS ONE. 2014a; 9:e108961. [PubMed: 25268775]

Mielcarek M, Inuabasi L, Bondulich MK, Muller T, Osborne GF, Franklin SA, Smith DL, Neueder A, Rosinski J, Rattray I, et al. Dysfunction of the CNS-heart axis in mouse models of Huntington's disease. PLoS Genet. 2014b; 10:e1004550. [PubMed: 25101683]

Mihm MJ, Amann DM, Schanbacher BL, Altschuld RA, Bauer JA, Hoyt KR. Cardiac dysfunction in the R6/2 mouse model of Huntington's disease. Neurobiol Dis. 2007; 25:297–308. [PubMed: 17126554]

Myers, RH., Marans, K., MacDonald, ME. Huntington's Disease In Genetic Instabilities and Hereditary Neurological Diseases. Warren, ST., Wells, RT., editors. The University of Michigan: Academic Press; 1998. p. 301-323.

Norton GR, Woodiwiss AJ, Gaasch WH, Mela T, Chung ES, Aurigemma GP, Meyer TE. Heart failure in pressure overload hypertrophy. The relative roles of ventricular remodeling and myocardial dysfunction. J Am Coll Cardiol. 2002; 39:664–671. [PubMed: 11849866]

Pattison JS, Sanbe A, Maloyan A, Osinska H, Klevitsky R, Robbins J. Cardiomyocyte expression of a polyglutamine preamyloid oligomer causes heart failure. Circulation. 2008; 117:2743–2751. [PubMed: 18490523]

Puthanveetil P, Wan A, Rodrigues B. FoxO1 is crucial for sustaining cardiomyocyte metabolism and cell survival. Cardiovasc Res. 2013; 97:393–403. [PubMed: 23263330]

Ravikumar B, Vacher C, Berger Z, Davies JE, Luo S, Oroz LG, Scaravilli F, Easton DF, Duden R, O'Kane CJ, Rubinsztein DC. Inhibition of mTOR induces autophagy and reduces toxicity of polyglutamine expansions in fly and mouse models of Huntington disease. Nat Genet. 2004; 36:585–595. [PubMed: 15146184]

Ribchester RR, Thomson D, Wood NI, Hinks T, Gillingwater TH, Wishart TM, Court FA, Morton AJ. Progressive abnormalities in skeletal muscle and neuromuscular junctions of transgenic mice expressing the Huntington's disease mutation. Eur J Neurosci. 2004; 20:3092–3114. [PubMed: 15579164]

Rosas HD, Goodman J, Chen YI, Jenkins BG, Kennedy DN, Makris N, Patti M, Seidman LJ, Beal MF, Koroshetz WJ. Striatal volume loss in HD as measured by MRI and the influence of CAG repeat. Neurology. 2001; 57:1025–1028. [PubMed: 11571328]

Sancak Y, Peterson TR, Shaul YD, Lindquist RA, Thoreen CC, Bar-Peled L, Sabatini DM. The Rag GTPases bind raptor and mediate amino acid signaling to mTORC1. Science. 2008; 320:1496–1501. [PubMed: 18497260]

Schilling G, Becher MW, Sharp AH, Jinnah HA, Duan K, Kotzuk JA, Slunt HH, Ratovitski T, Cooper JK, Jenkins NA, et al. Intranuclear inclusions and neuritic aggregates in transgenic mice expressing a mutant N-terminal fragment of huntingtin. Hum Mol Genet. 1999; 8:397–407. [PubMed: 9949199]

Schroeder AM, Wang HB, Park S, Jordan MC, Gao F, Coppola G, Fishbein MC, Roos KP, Ghiani CA, Colwell CS. Cardiac dysfunction in the BACHD mouse model of Huntington's disease. PLoS ONE. 2016; 11:e0147269. [PubMed: 26807590]

Sharma KR, Romano JG, Ayyar DR, Rotta FT, Facca A, Sanchez-Ramos J. Sympathetic skin response and heart rate variability in patients with Huntington disease. Arch Neurol. 1999; 56:1248–1252. [PubMed: 10520941]

She P, Zhang Z, Marchionini D, Diaz WC, Jetton TJ, Kimball SR, Vary TC, Lang CH, Lynch CJ. Molecular characterization of skeletal muscle atrophy in the R6/2 mouse model of Huntington's disease. Am J Physiol Endocrinol Metab. 2011; 301:E49–E61. [PubMed: 21505144]

Shende P, Plaisance I, Morandi C, Pellieux C, Berthonneche C, Zorzato F, Krishnan J, Lerch R, Hall MN, Rüegg MA, et al. Cardiac raptor ablation impairs adaptive hypertrophy, alters metabolic gene expression, and causes heart failure in mice. Circulation. 2011; 123:1073–1082. [PubMed: 21357822]

Song X, Kusakari Y, Xiao CY, Kinsella SD, Rosenberg MA, Scherrer-Crosbie M, Hara K, Rosenzweig A, Matsui T. mTOR attenuates the inflammatory response in cardiomyocytes and prevents cardiac

dysfunction in pathological hypertrophy. Am J Physiol Cell Physiol. 2010; 299:C1256–C1266. [PubMed: 20861467]

Sørensen SA, Fenger K. Causes of death in patients with Huntington's disease and in unaffected first degree relatives. J Med Genet. 1992; 29:911–914. [PubMed: 1479606]

Stanek LM, Yang W, Angus S, Sardi PS, Hayden MR, Hung GH, Bennett CF, Cheng SH, Shihabuddin LS. Antisense oligonucleotide-mediated correction of transcriptional dysregulation is correlated with behavioral benefits in the YAC128 mouse model of Huntington's disease. J Huntingtons Dis. 2013; 2:217–228. [PubMed: 25063516]

Tamai T, Yamaguchi O, Hikoso S, Takeda T, Taneike M, Oka T, Oyabu J, Murakawa T, Nakayama H, Uno Y, et al. Rheb (Ras homologue enriched in brain)-dependent mammalian target of rapamycin complex 1 (mTORC1) activation becomes indispensable for cardiac hypertrophic growth after early postnatal period. J Biol Chem. 2013; 288:10176–10187. [PubMed: 23426372]

The Huntington's Disease Collaborative Research Group. A novel gene containing a trinucleotide repeat that is expanded and unstable on Huntington's disease chromosomes. Cell. 1993; 72:971–983. [PubMed: 8458085]

Toczek M, Zielonka D, Zukowska P, Marcinkowski JT, Slominska E, Isalan M, Smolenski RT, Mielcarek M. An impaired metabolism of nucleotides underpins a novel mechanism of cardiac remodeling leading to Huntington's disease related cardiomyopathy. Biochim Biophys Acta. 2016; 1862:2147–2157. [PubMed: 27568644]

Trottier Y, Devys D, Imbert G, Saudou F, An I, Lutz Y, Weber C, Agid Y, Hirsch EC, Mandel JL. Cellular localization of the Huntington's disease protein and discrimination of the normal and mutated form. Nat Genet. 1995; 10:104–110. [PubMed: 7647777]

Uhlén M, Fagerberg L, Hallström BM, Lindskog C, Oksvold P, Mardinoglu A, Sivertsson Å, Kampf C, Sjöstedt E, Asplund A, et al. Proteomics. Tissue-based map of the human proteome. Science. 2015; 347:1260419. [PubMed: 25613900]

Walker FO. Huntington's disease. Lancet. 2007; 369:218–228. [PubMed: 17240289]

Wang M, Weiss M, Simonovic M, Haertinger G, Schrimpf SP, Hengartner MO, von Mering C. PaxDb, a database of protein abundance averages across all three domains of life. Mol Cell Proteomics. 2012; 11:492–500. [PubMed: 22535208]

Wang JJ, Rau C, Avetisyan R, Ren S, Romay MC, Stolin G, Gong KW, Wang Y, Lusis AJ. Genetic dissection of cardiac remodeling in an isoproterenol-induced heart failure mouse model. PLoS Genet. 2016; 12:e1006038. [PubMed: 27385019]

Wexler NS, Lorimer J, Porter J, Gomez F, Moskowitz C, Shackell E, Marder K, Penchaszadeh G, Roberts SA, Gayán J, et al. U.S.-Venezuela Collaborative Research Project. Venezuelan kindreds reveal that genetic and environmental factors modulate Huntington's disease age of onset. Proc Natl Acad Sci USA. 2004; 101:3498–3503. [PubMed: 14993615]

Wilhelm M, Schlegl J, Hahne H, Gholami AM, Lieberenz M, Savitski MM, Ziegler E, Butzmann L, Gessulat S, Marx H, et al. Mass-spectrometry-based draft of the human proteome. Nature. 2014; 509:582–587. [PubMed: 24870543]

Wood NI, Sawiak SJ, Buonincontri G, Niu Y, Kane AD, Carpenter TA, Giussani DA, Morton AJ. Direct evidence of progressive cardiac dysfunction in a transgenic mouse model of Huntington's disease. J Huntingtons Dis. 2012; 1:57–64. [PubMed: 24339845]

Yan L, Findlay GM, Jones R, Procter J, Cao Y, Lamb RF. Hyperactivation of mammalian target of rapamycin (mTOR) signaling by a gain-of-function mutant of the Rheb GTPase. J Biol Chem. 2006; 281:19793–19797. [PubMed: 16728407]

Zhang D, Contu R, Latronico MV, Zhang J, Rizzi R, Catalucci D, Miyamoto S, Huang K, Ceci M, Gu Y, et al. MTORC1 regulates cardiac function and myocyte survival through 4E-BP1 inhibition in mice. J Clin Invest. 2010; 120:2805–2816. [PubMed: 20644257]

Highlights

- Cardiac mHTT expression impairs mTORC1 activity in HD mouse model hearts
- Restoring cardiac mTORC1 activity in HD mice permits cardiac stress adaptation
- Chronic cardiac mTORC1 inhibition is cell-intrinsic, caused by Rheb mislocalization

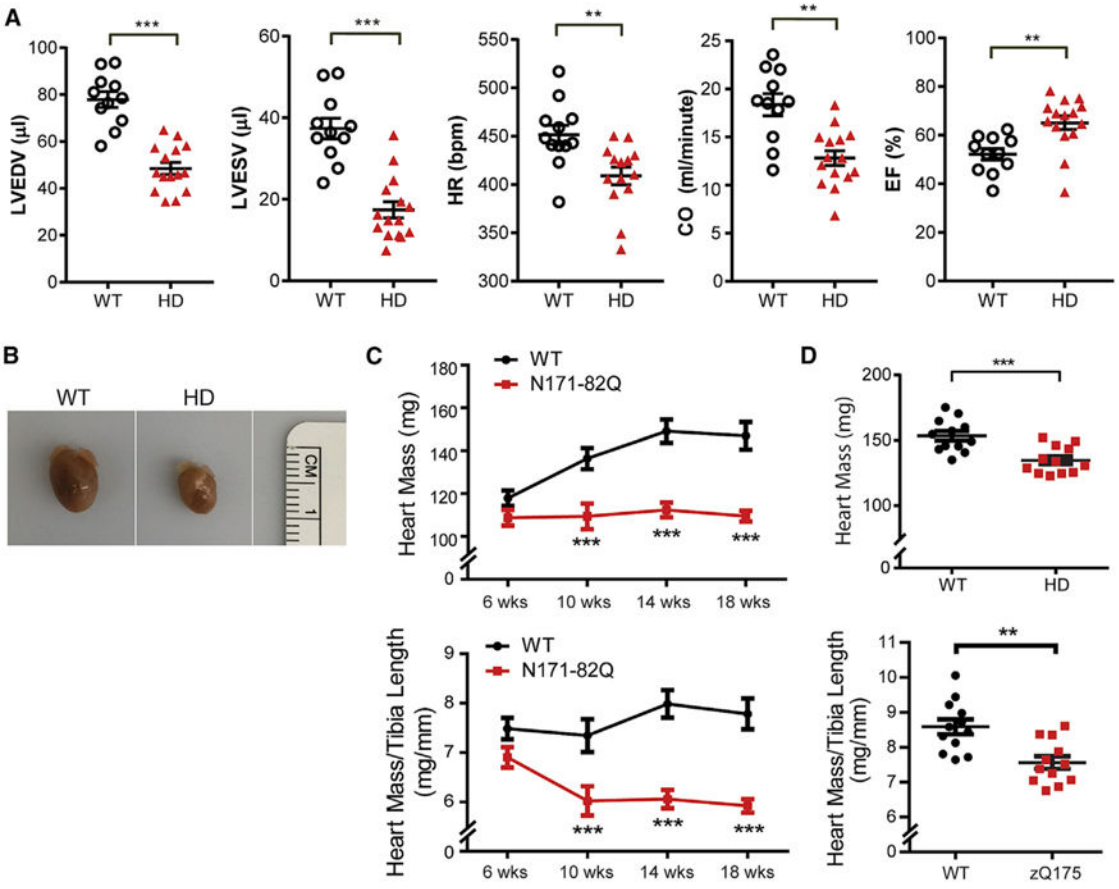

Figure 1.

Characterization of Heart Phenotype in N171-82Q and zQ175 Mouse Models Shows Decreased Mass but Normal Function

(A) Left ventricular volume measurements obtained by transthoracic echocardiography on 16-week-old male N171-82Q mice (late-stage disease). LVEDV, left ventricular end diastolic volume; LVESV, left ventricular end systolic volume; HR (bpm), heart rate (beats per min); CO, cardiac output; EF, ejection fraction. n ≥ 12 for both groups.

(B) Juxtaposed hearts from WT and N171-82Q mice showing gross size differences at 18 weeks of age.

(C) Growth curves of heart mass and heart mass normalized to tibia of N171-82Q male mice at 6 weeks (presymptomatic, n R 6), 10 weeks (early-stage disease, n R 10), 14 weeks (mid-stage disease, n R 8), and 18 weeks (late-stage disease, n R 8) of age.

(D) Heart mass and heart mass normalized to tibia length of zQ175 male mice at 12 months of age (post-symptomatic, n R 12).

Student's t test, *p ≤ 0.05; **p ≤ 0.01; ***p ≤ 0.001. Error bars represent SEM. See also Figure S1.

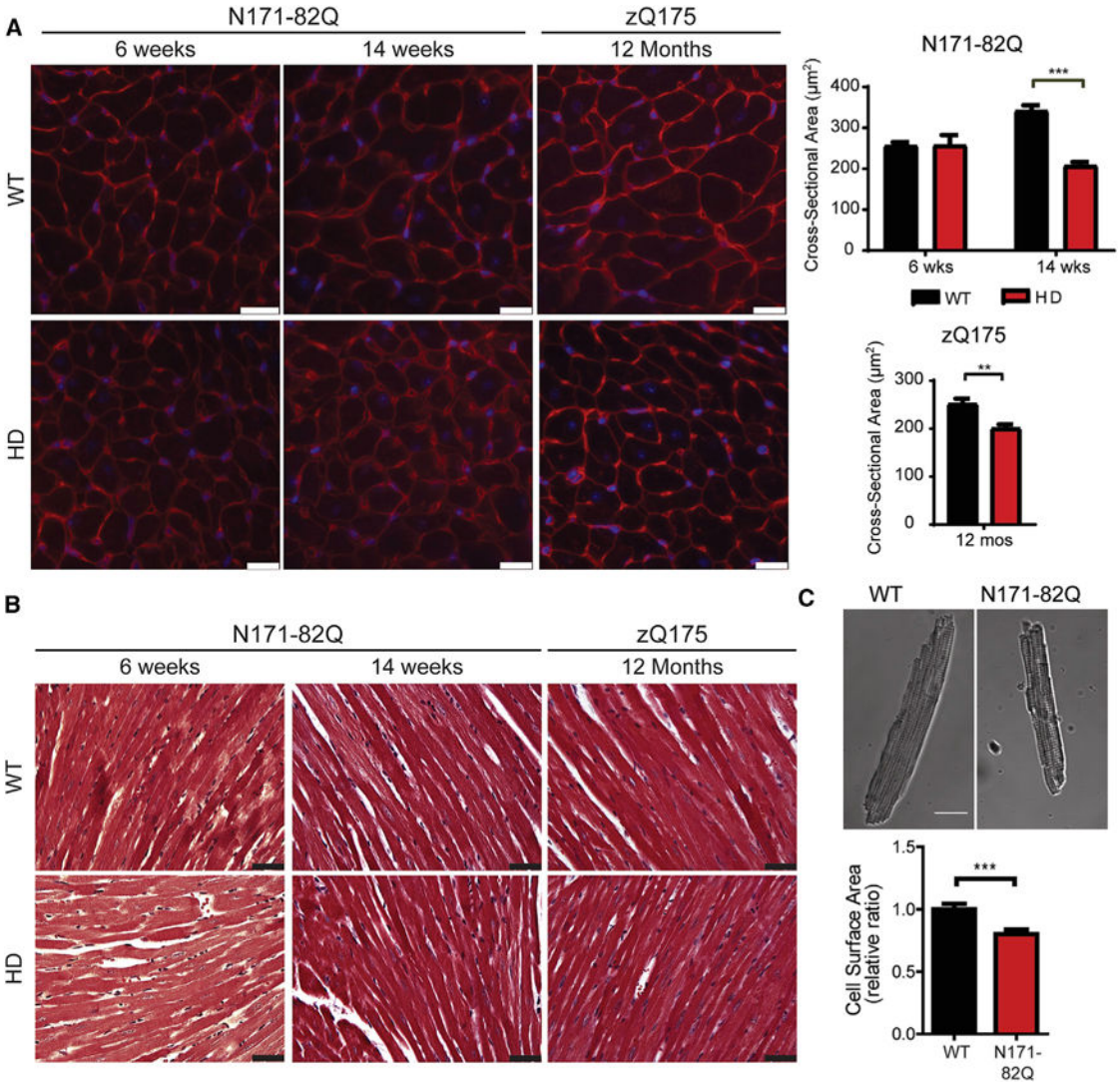

Figure 2.

HD Mouse Hearts Have Decreased Cardiomyocyte Size but No Fibrosis

(A) Wheat germ agglutinin staining and corresponding cardiomyocyte cross-sectional area measurements in N171-82Q mice at 6 ($n \geq 4$) and 14 ($n \geq 6$) weeks of age and zQ175 mice at 12 months of age ($n \geq 7$). Cardiomyocytes measured are from left ventricular posterior wall. Scale bars, 20 μm. $n \geq 200$ cells/heart.

(B) Masson's trichrome staining in left ventricle of hearts from N171-82Q at 6 weeks ($n \geq 6$) and 14 weeks ($n \geq 7$) of age and zQ175 mice at 12 months of age ($n \geq 10$). Nuclei stain black, proteins stain red, and collagen stains bright blue (not observed). Scale bars, 40 μm.

(C) Transillumination confocal image of isolated adult cardiomyocytes from 13-week-old WT and N171-82Q mice. Mean cell surface area is expressed relative to control WT (WT: n = 30 cells; N171-82Q: n = 27 cells; from 3 mice per group).

Student's t test, *$p \leq 0.05$; **$p \leq 0.01$; ***$p \leq 0.001$. Error bars represent SEM. See also Figure S1.

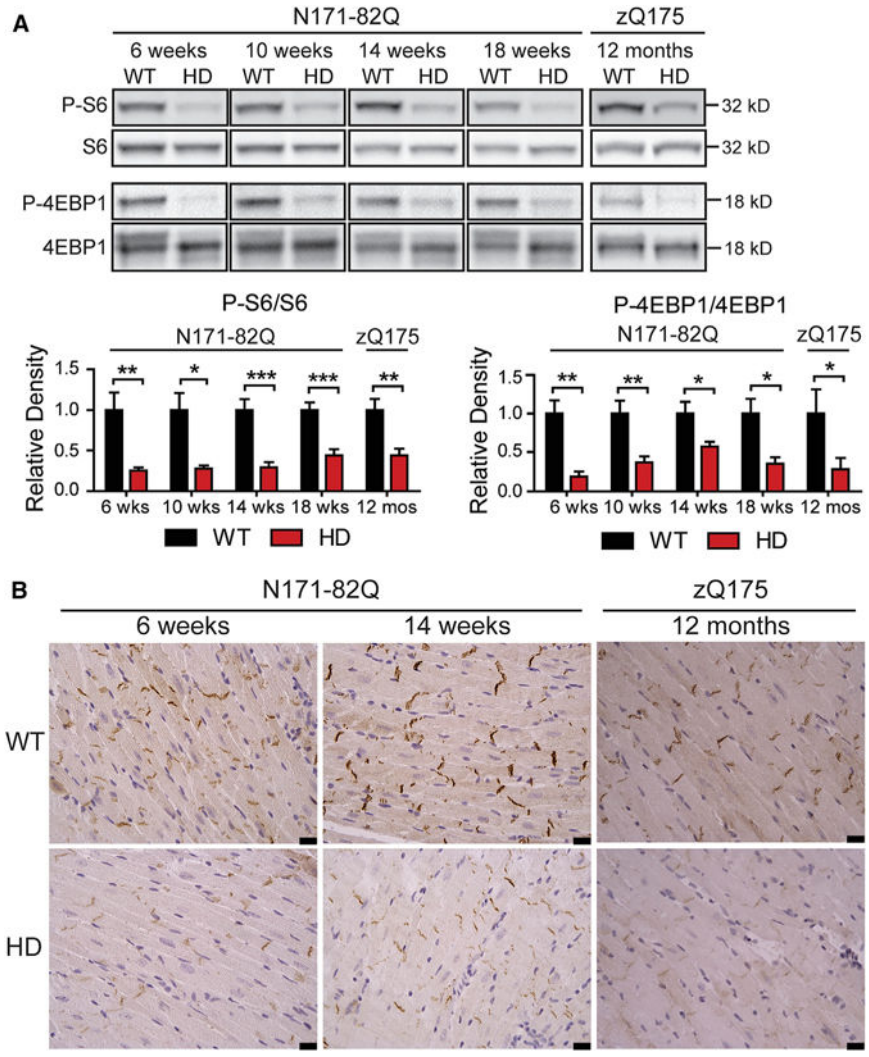

Figure 3.

Cardiac mTORC1 Activity Is Dysregulated in HD Murine Models

(A) Representative lanes and quantification of western blot analysis of heart lysates from N171-82Q mice at 6 ($n \geq 6$), 10 ($n \geq 7$), 14 ($n \geq 8$), and 18 ($n \geq 8$) weeks of age, and from zQ175 mice at 12 months of age ($n \geq 10$). Graphs represent mean band densities from phospho-specific antibodies normalized to band densities of phospho-independent antibodies and are expressed relative to WT levels. Student's t test, *$p \leq 0.05$; **$p \leq 0.01$; ***$p \leq 0.001$. Error bars represent SEM.

(B) Representative photomicrographs showing immunohistochemical staining for P-S6 in N171-82Q and WT littermate hearts at 6 weeks ($n \geq 5$) and 14 weeks ($n \geq 7$) of age and in zQ175 and WT littermate hearts at 12 months of age ($n \geq 10$). P-S6 stains brown. Scale bars, 20 μm.

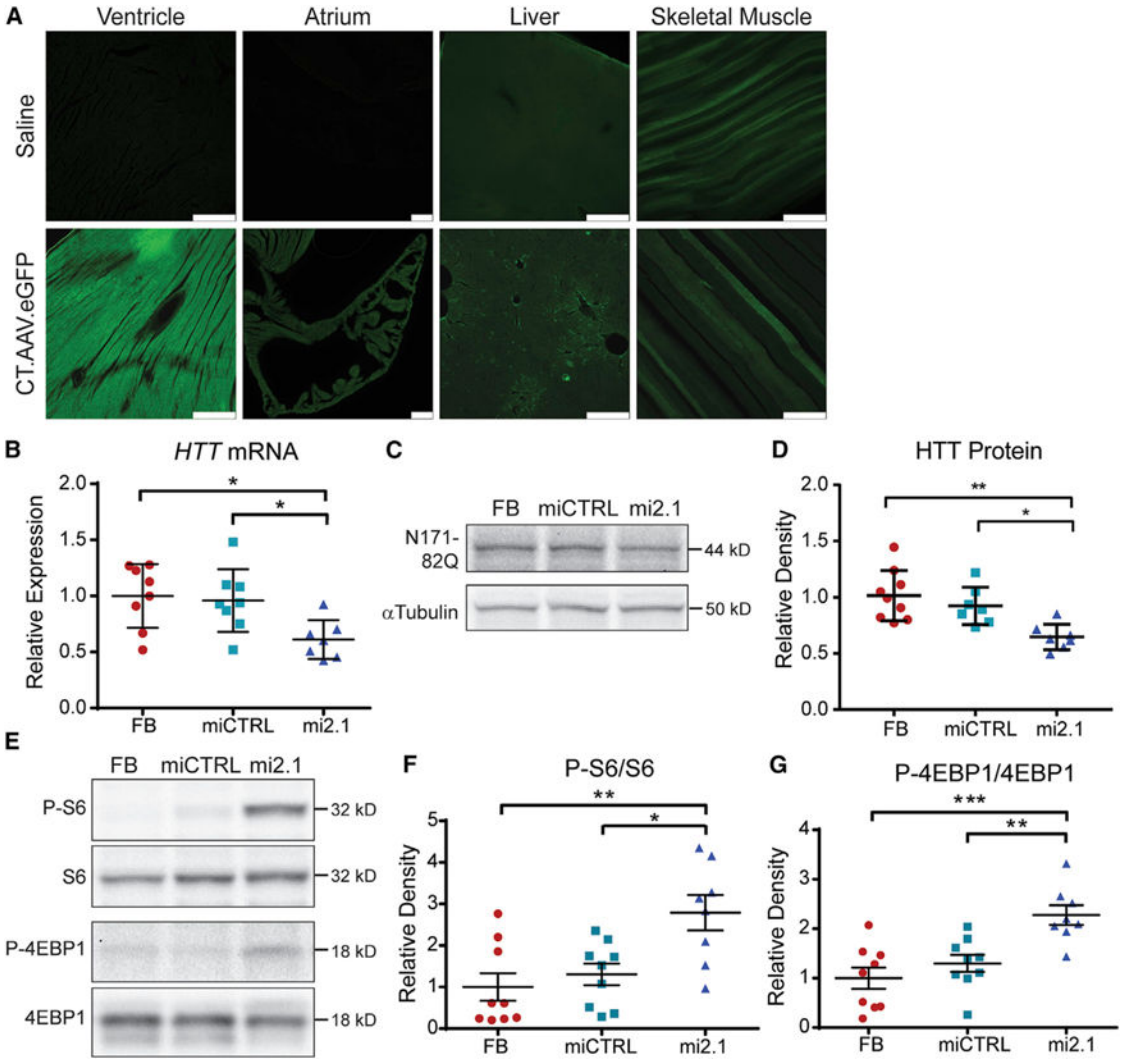

Figure 4.

RNAi-Mediated mHTT Knock Down Restores mTORC1 Activity in N171-82Q Mice

(A) Representative images depicting biodistribution of green fluorescence in WT mice systemically injected with either saline or CT.AAV.eGFP. n = 4 per group. Scale bars, 300 μm.

(B) Human *HTT* gene expression in knock down (KD) mouse hearts using CT.AAV as a vector. FB, formulation buffer; miCTRL, miRNA control; mi2.1, *HTT*-targeting miRNA. Expression levels were determined by standard curve, and graphs represent expression relative to FB controls. n ≥ 7 for each group. (C and D) Representative WB (C) and quantitation (D) for N171-82Q transgene expression in hearts from mice injected with FB or CT.AAV expressing miCTRL or mi2.1. Band densities were normalized to α-tubulin densities and graphed relative to FB samples. n ≥ 7 for each group. (E–G) Representative western blot (E) and quantitation of P-S6/S6 (F) and P-4EBP1/4EBP1 (G) in N171-82Q mice injected with FB or CT.AAV expressing miCTRL or mi2.1. Data are graphed relative to FB samples. n ≥ 7 for each group.

For (B)–(G), one-way ANOVA with Tukey's post hoc analysis, *p ≤ 0.05; **p ≤ 0.01; ***p ≤ 0.001. Error bars represent SEM.

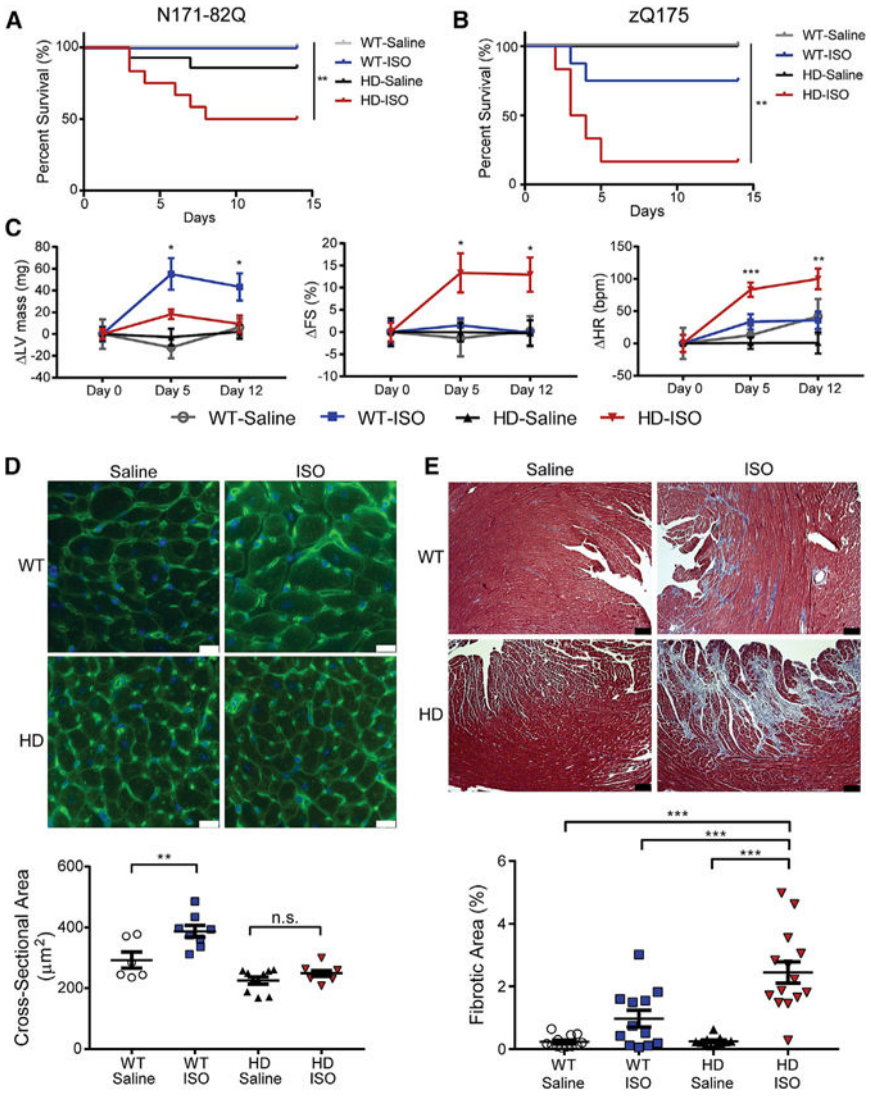

Figure 5.

Adaptive Response to Cardiac Stress Is Impaired in N171-82Q Mice

(A) Mortality in N171-82Q and WT littermates treated with isoprenaline (ISO) or saline for 14 days. n ≥ 8 for all groups.

(B) Mortality in zQ175 and WT littermates treated with ISO or saline for 14 days. n ≥ 7 for all groups.

(C) Transthoracic echocardiography measurements of left ventricular mass (LV Mass), fractional shortening (FS), and heart rate (HR) in N171-82Q and WT littermates after ISO or saline infusion for 0, 5, and 12 days. Graphs represent changes from pre-treatment baseline. n ≥ 5 for all groups.

(D) Representative wheat germ agglutinin staining of ISO- or saline-treated N171-82 and WT heart sections and measurement of left ventricular posterior wall cardiomyocyte mean cross-sectional area. N ≥ 6 hearts/group, n R 200 cells/heart. Scale bars, 20 μm.

(E) Masson's trichrome stain in representative heart sections from ISO- or saline-treated N171-82Q and WT littermates with quantitation of respective picrosirius red-stained

sections. Representative images show subendocardial region of left ventricle. N R 12 hearts for all groups, n ≥ 9 images analyzed/heart. Areas of fibrosis stain blue. Scale bars, 100 μm. Mantel-Cox (log-rank) test (A and B), one-way ANOVA with Sidak's multiple comparison analysis (C) or Tukey's post hoc analysis (D and E), *p ≤ 0.05; **p ≤ 0.01; ***p ≤ 0.001. Error bars represent SEM. See also Figure S2.

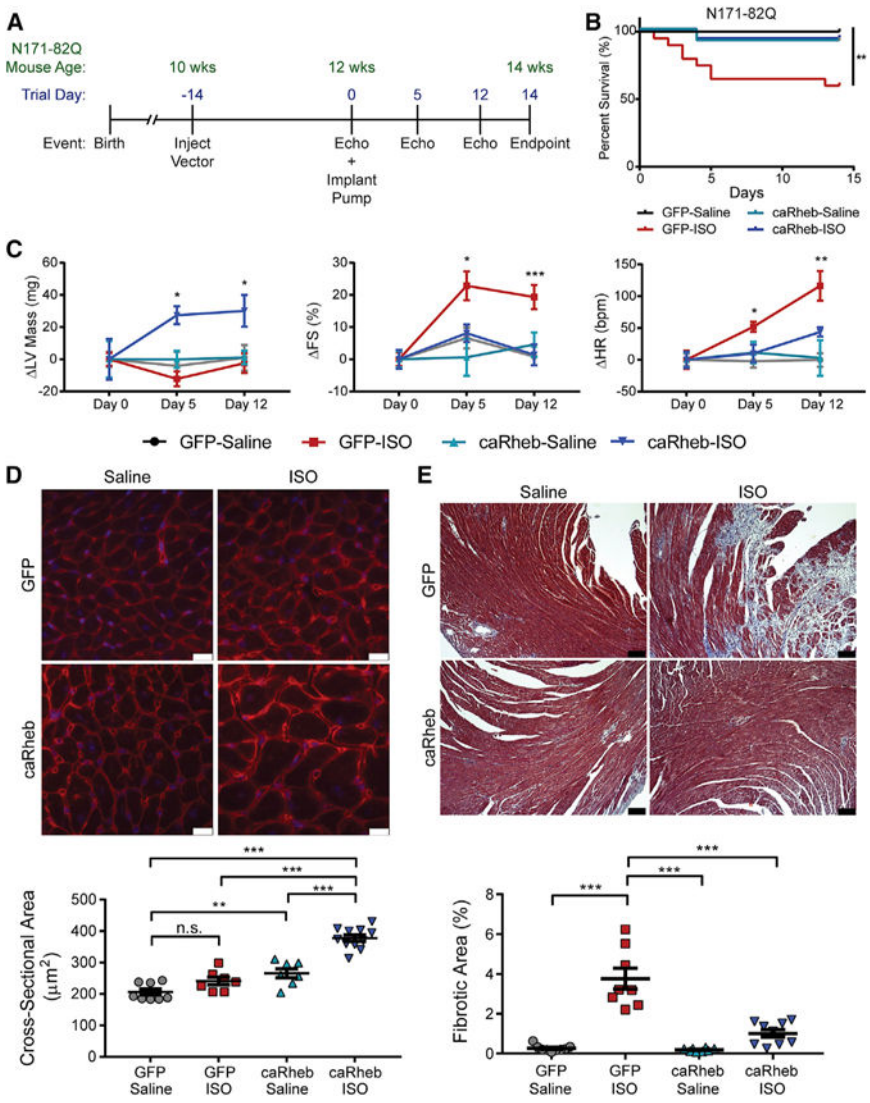

Figure 6.

mTORC1 Activation Restores Cardiac Stress Response Capability in N171-82Q Mice

(A) Experiment timeline.

(B) Mortality in N171-82Q mice (no WT) injected with CT.AAV expressing either GFP or constitu-tively active Rheb (caRheb), followed by treated with either isoprenaline (ISO) or saline for 14 days. n ≥ 12 for all groups.

(C) Transthoracic echocardiography assessments of left ventricular mass (LV mass), fractional shortening (FS), and heart rate (HR) in N171-82Q mice transduced with either CT.AAV.caRheb or CT.AAV.GFP after ISO or saline infusion for 0, 5, or 12 days. Graphs represent change from pretreatment baseline. n ≥ 4 for all groups.

(D) Representative wheat germ agglutinin stained-sections and measurement of left ventricular posterior wall cardiomyocyte mean cross-sectional area from N171-82Q hearts transduced with GFP or caRheb and treated with ISO or saline. N ≥ 8 hearts for all groups, n R 200 cells/heart.

(E) Masson’s trichrome stain in representative heart sections from ISO- or saline-treated N171-82Q mice transduced with either GFP or caRheb with quantitation of corresponding picrosirius red-stained sections. Representative images show subendocardial region of left ventricle. Areas of fibrosis stain blue. N ≥ 8 hearts for all groups, n ≥ 9 images analyzed/heart. Scale bars, 100 μm.

Mantel-Cox (log-rank) test (B), one-way ANOVA with Sidak’s multiple comparison analysis (C), or Tukey’s post hoc analysis (D and E), *p % 0.05; **p % 0.01; ***p % 0.001. Error bars represent SEM. See also Figure S3.

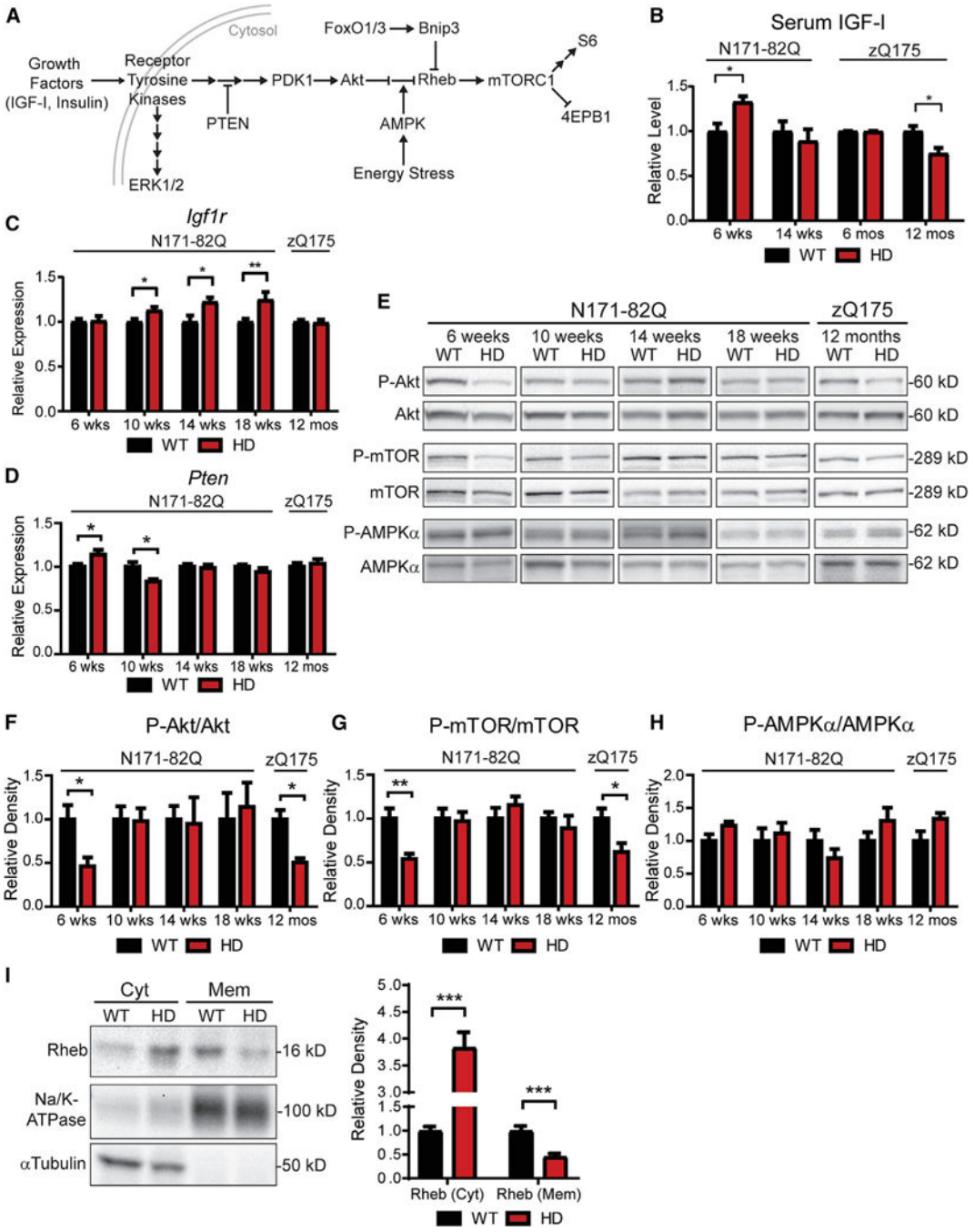

Figure 7.

Analysis of Upstream mTORC1 Pathway Signaling in HD Mouse Hearts

(A) Simplified schematic of mTORC1 activation pathway. Arrowheads represent activation step; blunted lines indicate inhibitory step. Some steps are not explicitly listed and are represented by multiple arrows.

(B) IGF-I levels in mouse serum from N171-82Q mice at 6 weeks ($n \geq 5$) and 14 weeks ($n \geq 7$) of age and from zQ175 mice at 6 months ($n \geq 5$) and 12 months of age ($n \geq 12$). Data are expressed relative to WT for each time point.

(C) *Igf1r* expression measured by qPCR in N171-82Q mice at 6 (n ≥ 6), 10 (n ≥ 7), 14 (n ≥ 8), and 18 (n ≥ 8) weeks of age, and in zQ175 mice at 12 months of age (n ≥ 10). *Igf1r* expression levels were normalized to *Tbp* expression as an internal control and are graphed relative to WT levels.
(D) *Pten* expression in N171-82Q mice at 6 (n ≥ 6), 10 (n ≥ 7), 14 (n ≥ 8), and 18 (n ≥ 8) weeks of age, and in zQ175 mice at 12 months of age (n ≥ 10), measured by qPCR. Gene expression levels were normalized to expression of *Tbp* mRNA as an internal control and are graphed relative to WT levels. (E) Representative blots of N171-82Q mice at 6 (n ≥ 6), 10 (n ≥ 7), 14 (n ≥ 8), and 18 (n ≥ 8) weeks of age, and from zQ175 mice at 12 months of age (n ≥ 10). (F–H) Graphs for (F) P-Akt/Akt, (G) P-mTOR/mTOR, and (H) P-AMPKa/AMPKa represent quantitation of band densities for phospho-specific antibodies normalized to band densities of phospho-independent antibodies and are expressed relative to WT levels.
(I) Representative western blot and quantitation from membrane purification of 16 week-old N171-82Q hearts. Loading controls were a-tubulin for cytoplasmic fractions, Na/K-ATPase for membrane fractions. For each group n = 6. Graphs represent Rheb density normalized to loading control from the corresponding lane and are expressed relative to WT.
For all panels, Student's t test, *p ≤ 0.05, **p ≤ 0.01, ***p ≤ 0.001. Error bars represent SEM. See also Figures S4–S6.